A LETTERS JOURNAL EXPLORING THE FRONTIERS OF PHYSICS

OFFPRINT

Bimodal range distributions of low-energy carbon ions in tetrahedral amorphous carbon

P. Neumaier, A. Bergmaier, W. Eckstein, R. Fischer, H. Hofsäss, H. U. Jäger, H. Kröger, C. Ronning and G. Dollinger

EPL, **90** (2010) 46002

A Letters Journal Exploring the Frontiers of Physics

May 2010

EPL, **90** (2010) 46002 www.epljournal.org
doi: 10.1209/0295-5075/90/46002

Bimodal range distributions of low-energy carbon ions in tetrahedral amorphous carbon

P. Neumaier[1], A. Bergmaier[2], W. Eckstein[3], R. Fischer[3], H. Hofsäss[4], H. U. Jäger[5], H. Kröger[4], C. Ronning[4] and G. Dollinger[2(a)]

[1] *Technische Universität München, Physik Department E12 - D-85748 Garching, Germany, EU*
[2] *Universität der Bundeswehr München, Angewandte Physik und Messtechnik, LRT 2 - D-85577 Neubiberg, Germany, EU*
[3] *Centre for Interdisciplinary Plasma Science, Max-Planck-Institut für Plasmaphysik, EURATOM Association Boltzmannstr. 2, D-85748 Garching, Germany, EU*
[4] *Universität Göttingen, II. Physikalisches Institut - Tammannstrasse 1-37077 Göttingen, Germany, EU*
[5] *Forschungszentrum Rossendorf e. V., Institut für Ionenstrahlphysik und Materialforschung - Postfach 510119, D-01314 Dresden, Germany, EU*

received 8 December 2009; accepted in final form 4 May 2010
published online 4 June 2010

PACS 68.55.A- – Nucleation and growth
PACS 81.15.Aa – Theory and models of film growth
PACS 81.05.U- – Carbon/carbon-based materials

Abstract – Range and mixing distributions of carbon ions deposited onto tetrahedral amorphous carbon films at kinetic energies between 22 eV and 692 eV are measured utilizing high-resolution elastic recoil detection. These data are compared to respective calculations based on binary collision approximation as well as to classical molecular-dynamics simulations. The measured range profiles reveal asymmetric, bimodal structures which are not reproduced from theories. The measured mixing distributions approve the measured range distributions, in particular the observed differences between theory and experiment, which have to be considered in subplantation growth models.

Bombardment of surfaces by hyperthermal but low-energy (≈1–1000 eV) ions significantly changes the properties of any material within the range of the impinging ions. The ion impact initiates non-equilibrium processes that offer the possibility to grow materials with new, unique structures and properties. The most prominent example, tetrahedral amorphous carbon (ta–C), is a form of amorphous carbon with a predominant tetrahedral configuration which means diamond-type carbon–carbon bonds with sp^3 hybridisation. An sp^3 fraction exceeding 80% was reported [1,2]. It can only be grown by depositing carbon ions at ≈50–1000 eV [3–5]. The structure of this material and the crucial role of the ion energy in tuning the properties of the evolving carbon films between those of graphite and diamond was subject to a series of experimental studies [2,6–11]. Subplantation, which is the implantation of the film forming atomic species below the actual surface, was early recognised as being the basic mechanism promoting sp^3 bonds and a large carbon density of about 3 g/cm^3 [1,3,12]. According to Lifshitz *et al.* the ion impact affects processes on three different time scales [3,12]: i) a collisional stage where the impinging ions transfer their energy in mainly two-body collisions to the target atoms within time scales below 10^{-13} s, ii) a short ($<10^{-11}$ s) thermalization stage where the stopped ion and the surrounding excited atoms thermalize and cool down (thermal spike concept), and iii) a long-term relaxation stage ($>10^{-10}$ s) where still some rearrangement of the atoms may occur. The problem for theories is the complexity due to the many-particle problem which has to be solved over many orders of magnitude in energy and time scales. Molecular-dynamics (MD) simulations have achieved considerable progress in recent studies [13–15]. In addition, a number of analytical descriptions have been developed to describe the experimental findings [1,3,12,16–19]. However, the details of ta–C growth, in particular the importance of the different time stages for the initiation of sp^3 bonds are still under debate.

(a) E-mail: guenther.dollinger@unibw.de

In this work we report the first measurement of range distributions of carbon ions implanted into amorphous carbon at energies which are relevant for ta–C growth. These data are compared to calculated range distributions based on binary collisions containing only stage i) of the subplantation and to classical MD calculations which extend the considered atomic interactions in the solid up to stage ii). Significant differences between measurement and calculation emerge for the range distributions. These differences are confirmed by mixing distributions measured from carbon marker layers. The experiment delivers new experimental data for the interaction of low-energy ions with solids which allow for a crucial test for models of the subplantation scheme and may serve as a base for improved calculations.

Two different classes of amorphous carbon films are grown using mass-selected ion-beam deposition (MSIBD) at room temperature in UHV ($<1\times10^{-6}$ Pa) [20]: for the first class of films, initially about 12 nm ^{12}C are deposited onto sputter-cleaned Si (100) substrates at ion energies $E_{\rm ion}$ between 22 eV and 692 eV. $E_{\rm ion}$ is determined with an accuracy of ±8 eV. The amount of deposited C^+ ions is measured by the integrated beam current. Following ^{12}C deposition about 5×10^{14} at/cm^2 ^{13}C are implanted at the same energies $E_{\rm ion}$. The small amount of implanted ^{13}C is chosen in order to minimize mixing effects within the implantation profiles. The second class of samples is grown as described above, but with the distinction that finally another 9×10^{16} at/cm^2 ^{12}C (this corresponds to 6 nm at a mass density of 3 g/cm^3) are deposited with the same $E_{\rm ion}$. Using this procedure ta–C films are grown, that contain either directly on the surface or 6–9 nm beneath the surface 5×10^{14} at/cm^2 ^{13}C. The range distributions are measured using the films with the topmost ^{13}C layer, the mixing effects involved in ta–C growth are investigated using the films with the ^{13}C interfacial layer.

The ^{13}C depth profiles are analyzed by high-resolution elastic recoil detection (ERD). The experimental arrangement and the data analysis in the framework of Bayesian probability theory are described in ref. [21]. Beam damage is negligible utilizing a 40 MeV $^{197}Au^{19+}$ beam and scanning a 50 mm^2 target size at a fluence of about 1×10^{12} ions cm^{-2}. 40 MeV Au ions show a stopping power of $(798\pm12)\times10^{-15}$ eV at^{-1} cm^2 in transmission experiments through thin carbon foils. This value is used for any solid carbon modification since it has been shown that the stopping power for heavy ions at this velocity does not change significantly in different carbon modifications [22]. The measured stopping power allows for accurate conversion of the energy scale to a depth scale. It is given in units of at/cm^2 since the density profile close to the surface is not accurately known (*i.e.* 1×10^{16} at/cm$^2\equiv1$ nm at 2 g/cm^3). Utilizing an incident angle of 4° with respect to the surface and a scattering angle of 15° a depth resolution at the target surface of 3×10^{15} at/cm^2 (FWHM) is measured, which is better than a (002)-monolayer thickness in graphite. Energy loss distributions after 3×10^{15} at/cm^2 are Gaussian shaped since the energy loss of a 40 MeV ^{197}Au ion is much larger than the maximum energy transfer to a free electron in a single collision [23,24]. In particular, a Lewis effect [25] is not present for these analysing conditions. Small tails far below percent level are expected from plural scattering effects but they are below statistical significance in the present experiments. Experiments on ^{13}C/^{12}C multilayers [21] as well as the demonstration of single monolayer resolution in graphite [23] verifies the assumption of a Gaussian shape energy distribution already behind one monolayer (*i.e.* 3×10^{15} at/cm^2).

The measurements are performed at a pressure of 1×10^{-6} Pa inside the scattering chamber of the Q3D magnetic spectrograph. It is proven by ERD that the surfaces are contaminated with about 2×10^{14} at/cm^2 oxygen during measurement, which does not significantly disturb depth profiles even in the range of monolayer resolution. A homogeneous hydrogen content of about 2 at% is detected in the ta–C films. Other elemental content sums up to less than 10^{13} at/cm^2.

Figure 1(a)–(h) shows ^{13}C range profiles for ion energies between $E_{\rm ion}=22$ eV and $E_{\rm ion}=692$ eV. Zero depth in the spectra marks the surface of the carbon films and is determined from an independent measurement on a pure amorphous ^{13}C sample [21]. Its uncertainty is $\pm7\times10^{14}$ at/cm^2 (corresponding to ±0.7 Å at a supposed surface density of 2 g/cm^3). The shaded area in fig. 1(a)–(h) visualizes the uncertainty of the reconstructions (±1 standard deviation σ). The measured spectra reveal non-symmetric structures, steep rising slopes and flat shoulders towards the bulk. At $E_{\rm ion}\leqslant222$ eV a peak close to the surface and a second, broad structure at larger depth are revealed (fig. 1(a)–(f)). Even a double peak is reconstructed at $E_{\rm ion}=22$ eV and at $E_{\rm ion}=92$ eV (fig. 1(a) and (d)). Within the $\pm1\sigma$ confidence interval the double-peak structure at 92 eV is significant. The 22 eV profile is consistent with a smooth shoulder. The presence of a second structure beyond the surface peak is significant at all energies below 222 eV.

The measured range profiles are compared to range calculations carried out with the Monte Carlo program TRIM.SP [26], that is based on a binary collision model as well as using classical MD studies [15]. TRIM.SP calculations are performed for amorphous carbon at a density of 2.26 g/cm^3. In order to adjust the real energy deposition during ion impact we add the surface binding energy of 7 eV to each actual ion energy. Kinetic energy gain of the incoming ion due to image charge attraction being in the range of 1–2 eV [27] is neglected.

MD calculations are performed in two steps: 1) carbon substrates of 5–7 nm thickness are simulated by depositing 2500–3500 C atoms at $T=20$ °C on a {111} diamond supercell consisting of 12 atomic layers with 56 C atoms per layer [15] and 2) 500 independent C impacts onto the simulated structure are considered at each energy in order to extract the range distributions. The atomic motions are

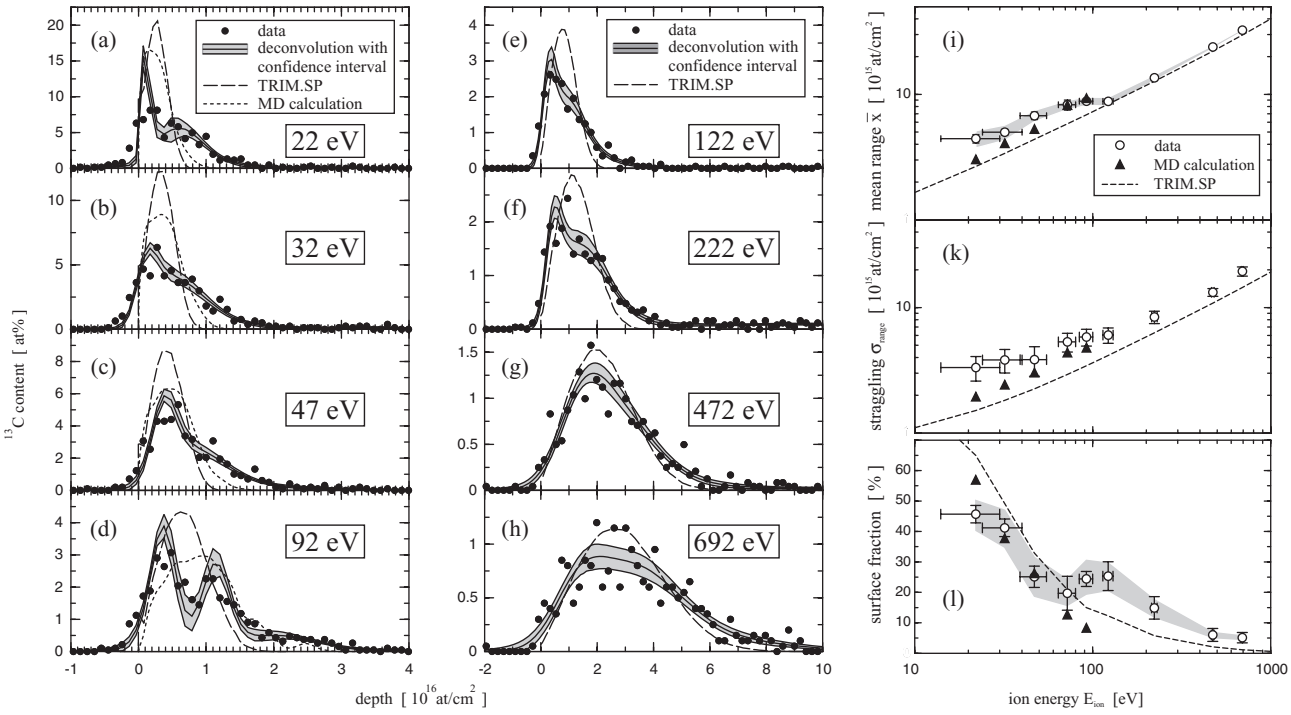

Fig. 1: (a)–(h) Measured and calculated range distributions of $^{13}C^+$ ions implanted at energies which are shown in the plot. The substrates are amorphous ^{12}C layers grown by mass-selected ion-beam deposition (MSIBD) at the same energies, respectively. (i) Measured and calculated mean ion ranges, (k) range straggling and (l) fraction of $^{13}C^+$ ions incorporated within the topmost 3×10^{15} at/cm^2.

followed for a relaxation time of 15 ps after every carbon ion impact. We use the analytical hydrocarbon potential of Brenner with improved C–C interaction cutoffs [15], electronic stopping is not included. The largest C^+ ion energy calculated is $E_{\rm ion} = 92\,{\rm eV}$ due to the high CPU time consumption.

Compared to the experimental data, TRIM.SP yields much narrower, more symmetric structures (fig. 1(a)–(h)). The non-symmetric shape of the measured profiles is better reconstructed by the MD simulation, although the calculated structures are narrower than the measured structures up to $E_{\rm ion} = 47\,{\rm eV}$ (fig. 1(a)–(d)). The bimodal structures and in particular the double-peak structure at $E_{\rm ion} = 92\,{\rm eV}$ are by no means reconstructed from both simulations.

Mean ion range $\bar{x}$, the range straggling $\sigma_{\rm range}$ (standard deviation) and the portion of ions found at film surface are evaluated for each spectrum $f(x)$ (fig. 1(i)–(l)). The measured ion ranges increase with energy except for a plateau around 100 eV, an energy region where the maximum sp^3 content is reported [9]. Besides this plateau an almost linear energy dependence of $\bar{x}$ is observed revealing a nearly constant stopping power ${\rm d}E/{\rm d}x \approx 24\,{\rm eV}/(10^{15}\,{\rm at/cm^2})$. Thus, an approximately uniform energy deposition along the ion track is obtained, which was assumed in recent studies [19]. Mean ion ranges being calculated with TRIM.SP match to the measured values at $E_{\rm ion} \geqslant 122\,{\rm eV}$ but are significantly too small at lower energies. The MD mean ranges reveal a steeper energy dependence below 100 eV but are in agreement with experimental data at $E_{\rm ion} \geqslant 72\,{\rm eV}$. The differences between the MD and TRIM.SP are attributed due to different carbon substrates, different interatomic potentials and thermal spike effects which are included within the MD but not within TRIM.SP.

The range straggling $\sigma_{\rm range}$ is depicted in fig. 1(k). TRIM.SP calculations show values that are significantly smaller than measured. The MD results are also smaller than measured but closer to experiment, the discrepancy between MD and measurement at $E_{\rm ion} \geqslant 47\,{\rm eV}$ is at the limit of significance.

Figure 1(l) shows the ^{13}C fraction found at the surface up to a thickness of 3×10^{15} at/cm^2. Best agreement with measurement is obtained at low energies for MD. The measured data reveal a significant plateau at about 100 eV which is in no way represented by theories.

The ion impact initiates a mixing of the carbon atoms. In order to analyze this mixing effect, ^{13}C depth profiles for the samples with the ^{13}C interfacial layer are measured. The atomic mixing is characterized via the alteration of the ^{13}C range profiles induced by subsequent ^{12}C bombardment. The measured ^{13}C mixing distributions shown in fig. 2 are much wider than the respective range profiles (fig. 1(b)–(h)).

Respective calculations are performed with the Monte Carlo program TRIDYN [28], as well as using the classical

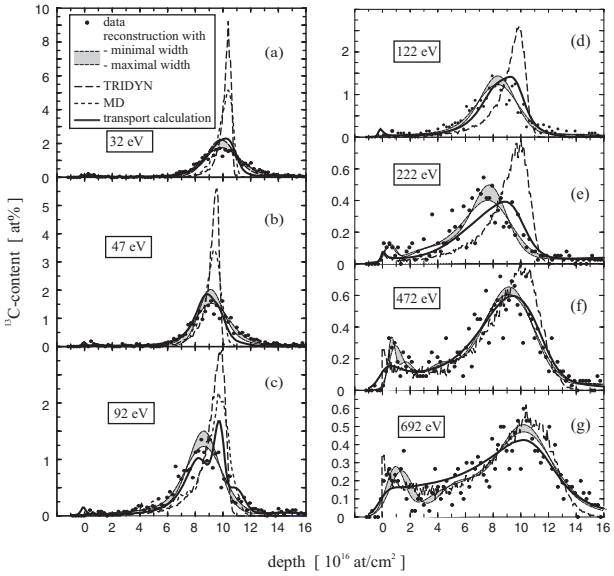

Fig. 2: Measured and calculated ^{13}C mixing distributions at ion energies which are shown in the plot. TRIDYN and transport calculations are carried out for a 9×10^{16} at/cm^2 thick ^{12}C cap layer. The MD simulation is performed for ion energies $E_{\text{ion}} \leqslant 92$ eV and a 5×10^{16} at/cm^2 thick ^{12}C cap layer due the high CPU time consumption.

MD studies [15]. TRIDYN is a dynamical version of TRIM.SP [26] which is capable to simulate ion beam deposition at large fluences, again considering only the collisional stage i) of the subplantation process. The MD simulations are restricted to $E_{\text{ion}} \leqslant 92$ eV and to a 5×10^{16} at/cm^2 thick ^{12}C cap layer due the high CPU time consumption. Additionally, mixing distributions are derived from a transport calculation based on the measured range distributions: ^{12}C is deposited successively appropriate to the measured range profiles and the density is relaxed instantaneously.

At energies below 222 eV the measured mixing profiles are clearly broader than the respective TRIDYN and MD calculations, but match the results from the transport calculation within the experimental uncertainties (fig. 2(a)–(e)). This approves the measured range distributions as well as the relevance of the observed discrepancies between the range profiles from theory and experiment. At energies above 472 eV the experiment is well reconstructed from TRIDYN simulations (fig. 2(f),(g)). Thus, the atomic mixing is dominated from effects of the collisional cascade at these high energies.

The observed differences between measurement and theories are mainly attributed to thermal spike effects: Range profiles are widened by atomic diffusion during the thermal spike (phase II) which develops due to the energy deposited in the ion track. This additional broadening can be calculated as a function of the thermal diffusivity D using the thermal spike model of ref. [19]. A smaller D value extends the duration of the spike and increases atomic diffusion. The broadening is negligible compared to the widths of the experimental range distributions if D is taken from literature for bulk ta–C, $D \approx 5 \times 10^{11}$ nm^2/s [19]. However, the experimental widths are well reproduced assuming 1/10 of this thermal diffusivity. Such a significantly reduced thermal diffusivity may be expected for the low-density, open carbon structure as it is calculated from quantum-mechanical molecular dynamics close to the surface of a ta–C structure [14]. In addition, the energy barrier for carbon self-diffusion being about 3 eV in ta–C may be reduced for the low-density surface near carbon structure which would lead to an enhanced atomic self-diffusion even at a larger thermal diffusivity.

In conclusion, we have measured range and mixing profiles of low-energy carbon ions as they are used in ta–C growth. With this new set of data, existing and forthcoming models can be tested regarding their success to describe ta–C growth. Actual microscopic theories show only partial agreement. With respect to macroscopic theories the measured range profiles can serve as detailed input. The experiments as presented here represent pilot experiments in order to get a deeper understanding within the large field of low-energy ion-solid interaction, like diamond nucleation, growth of cubic boron nitride, sputter erosion for depth profiling, ion polishing, or surface nanostructuring of various materials.

REFERENCES

[1] McKenzie D. R., Muller D. and Pailthorpe B. A., *Phys. Rev. Lett.*, **67** (1991) 773.
[2] Gaskell P. H. *et al.*, *Phys. Rev. Lett.*, **67** (1991) 1286.
[3] Lifshitz Y., Kasi S. R. and Rabalais J. W., *Phys. Rev. Lett.*, **62** (1989) 1290.
[4] Lifshitz Y., *Diam. Relat. Mater.*, **5** (1996) 388.
[5] Fallon P. J. *et al.*, *Phys. Rev. B*, **48** (1993) 4777.
[6] Lifshitz Y., Lempert G. D. and Grossman E., *Phys. Rev. Lett.*, **72** (1994) 2753.
[7] Kulik J. *et al.*, *Phys. Rev. B*, **52** (1995) 15812.
[8] Grossman E. *et al.*, *Appl. Phys. Lett.*, **68** (1996) 1214.
[9] Ronning C. *et al.*, *Diam. Relat. Mater.*, **6** (1997) 830.
[10] Davis C. A., Amaratunga G. A. J. and Knowles K. M., *Phys. Rev. Lett.*, **80** (1998) 3280.
[11] Zhao J. P. and Chen Z. J., *Phys. Rev. B*, **63** (2001) 115318.
[12] Lifshitz Y. *et al.*, *Phys. Rev. B*, **41** (1990) 10468.
[13] Kaukonen H. P. and Nieminen R. M., *Phys. Rev. Lett.*, **68** (1992) 620.
[14] Uhlmann S., Frauenheim Th. and Lifshitz Y., *Phys. Rev. Lett.*, **81** (1998) 641.
[15] Jäger H. U. and Albe K., *J. Appl. Phys.*, **88** (2000) 1129.
[16] Robertson J., *Diam. Relat. Mater.*, **2** (1993) 984.
[17] Davis C. A., *Thin Solid Films*, **226** (1993) 30.
[18] Koponen I., Hakovirta M. and Lappalainen R., *J. Appl. Phys.*, **78** (1995) 5837.
[19] Hofsäss H. *et al.*, *Appl. Phys. A*, **66** (1998) 153.
[20] Hofsäss H. *et al.*, *Diam. Relat. Mater.*, **3** (1994) 137.
[21] Neumaier P. *et al.*, *Nucl. Instrum. Methods B*, **183** (2001) 48.

[22] Baek W. Y. *et al.*, *Phys. Rev. A*, **35** (1987) 51.
[23] Dollinger G., Frey C. M., Bergmaier A. and Faestermann T., *Europhys. Lett.*, **42** (1998) 25.
[24] Schmelmer O., Dollinger G., Frey C. M., Bergmaier A. and Karsch S., *Nucl. Instrum. Methods B*, **145** (1998) 261.
[25] Lewis H. W., *Phys. Rev.*, **125** (1962) 937.
[26] Biersack J. P. and Eckstein W., *Appl. Phys. A*, **34** (1984) 73.
[27] Aumayr F. *et al.*, *Phys. Rev. Lett.*, **71** (1993) 1943.
[28] Möller W., Eckstein W. and Biersack J. B., *Comput. Phys. Commun.*, **51** (1988) 355.